ARMAX-Based Transfer Function Model Identification Using Wide-Area Measurement for Adaptive and Coordinated Damping Control

Hesen Liu, Lin Zhu, *Member, IEEE*, Zhuohong Pan, *Member, IEEE*, Feifei Bai, Yong Liu, *Member, IEEE*, Yilu Liu, *Fellow, IEEE*, Mahendra Patel, *Senior Member, IEEE*, Evangelos Farantatos, *Member, IEEE*, and Navin Bhatt, *Fellow, IEEE*

***Abstract*—One of the main drawbacks of the existing oscillation damping controllers that are designed based on offline dynamic models is adaptivity to the power system operating condition. With the increasing availability of wide-area measurements and the rapid development of system identification techniques, it is possible to identify a measurement-based transfer function model online that can be used to tune the oscillation damping controller. Such a model could capture all dominant oscillation modes for adaptive and coordinated oscillation damping control. This paper describes a comprehensive approach to identify a low-order transfer function model of a power system using a multi-input multi-output (MIMO) autoregressive moving average exogenous (ARMAX) model. This methodology consists of five steps: 1) input selection; 2) output selection; 3) identification trigger; 4) model estimation; and 5) model validation. The proposed method is validated by using ambient data and ring-down data in the 16-machine 68-bus Northeast Power Coordinating Council system. The results demonstrate that the measurement-based model using MIMO ARMAX can capture all the dominant oscillation modes. Compared with the MIMO subspace state space model, the MIMO ARMAX model has equivalent accuracy but lower order and improved computational efficiency. The proposed model can be applied for adaptive and coordinated oscillation damping control.**

***Index Terms*—Autoregressive moving average exogenous (ARMAX), correlation coefficient index, oscillation damping control, subspace state space, subspace state-space system identification (N4SID), system identification, transfer function model, wide-area measurement system (WAMS).**

Manuscript received March 10, 2015; revised June 18, 2015; accepted August 13, 2015. This work was supported in part by the Electric Power Research Institute, Engineering Research Center Shared Facilities through the Department of Energy under National Science Foundation Award Number EEC1041877, and in part by the CURENT Industry Partnership Program. Paper no. TSG-00284-2015.

H. Liu, L. Zhu, Z. Pan, and Y. Liu are with the Department of Electrical Engineering and Computer Science, University of Tennessee, Knoxville, TN 37996 USA (e-mail: zhlhustceee@gmail.com).

F. Bai is with the School of Electrical Engineering, Southwest Jiaotong University, Chengdu 610031, China, and also with the Department of Electrical Engineering and Computer Science, University of Tennessee, Knoxville, TN 37996 USA.

Y. Liu is with the Department of Electrical Engineering and Computer Science, University of Tennessee, Knoxville, TN 37996 USA, and also with the Oak Ridge National Laboratory, Oak Ridge, TN 37831 USA.

M. Patel, E. Farantatos, and N. Bhatt are with the Electric Power Research Institute, Palo Alto, CA 94304 USA.

Color versions of one or more of the figures in this paper are available online at http://ieeexplore.ieee.org.

Digital Object Identifier 10.1109/TSG.2015.2470648

I. Introduction

IN TODAY'S interconnected power grids, low-frequency oscillation is a significant issue limiting the power transfer capability and even deteriorating the power system security [1]. In order to suppress low-frequency oscillations, local and wide-area power system stabilizers (PSSs) are installed or proposed to provide supplementary damping control through generator excitation systems [2], flexible alternating current transmission systems (FACTS) devices [3], and high-voltage direct current (HVDC) links [4].

However, since these oscillation damping controllers are usually tuned based on several typical operating conditions, their performances may degrade if the actual operating condition is significantly different from the typical operating conditions considered in the offline design procedure. In some extreme cases, they even provide negative damping. Limited adaptivity is considered as one of the main drawbacks of these controllers.

A robust control scheme can be utilized to improve adaptivity. In general, a robust oscillation damping controller is designed based on a detailed system model under a selected dominant operating condition with bounded model uncertainty [5], [6]. The variations of operating condition are reflected in the additive and/or multiplicative uncertainty of the system model. Nevertheless, it is not easy to determine the uncertainty boundary of the system model. Additionally, the controller performance may not be optimal when the actual operating condition deviates from the dominant one.

An adaptive control scheme is another approach to improve adaptivity, which can update the controller parameters online to track the continuous variations in operating conditions. Recently, with the increasing application of the wide-area measurement system (WAMS) [7], [8] and the rapid development of system identification techniques [9], the adaptive control approach has drawn increasing attention. For instance, a self-tuning adaptive PSS based on artificial neural networks is proposed in [10]. In [11], the parameters of phase lead-lag compensators are updated based on the online modal analysis. However, most of the research focuses on the adaptivity of the individual damping controller, while the coordination among different controllers has not been fully addressed. If the system model depicting all the dominant oscillation modes is identified online, it is feasible to optimize the controllers'

parameters at the control center, and remotely configure the parameters of dispersed damping controllers. In this way, the adaptivity of the individual controller and the coordination among different oscillation modes can be achieved simultaneously [12].

Fast online identification of the system model to capture all oscillation modes (not a single mode) of the power system is the prerequisite of the adaptive and coordinated oscillation damping control. Two categories of measurement-based models can be used for system identification: 1) the subspace state space model and 2) the autoregressive moving average exogenous (ARMAX) model. The subspace state space model is usually identified by numerical algorithms for the subspace state-space system identification (N4SID) method [13]–[15] or the stochastic subspace identification method [16], [17]. However, the main drawback of these two approaches is slow computation speed due to singular value decomposition (SVD) of a large-dimensional matrix. Since the slow calculation speed is one of the barriers to apply the subspace state space model for oscillation damping control in the online environment, a recursive adaptive stochastic subspace identification method is presented in [17] to reduce the computation time.

The ARMAX model identification can be an alternative to overcome the drawback of high-computational burden [18], [19]. The family of autoregressive models has already been used to represent system dynamics for oscillation damping control [20], [21]. However, the identified ARMAX model is generally a single-input single-output (SISO) model, which may reflect only one oscillation mode because the model is used to control single oscillation mode.

This paper proposes a methodology to identify a multi-input multi-output (MIMO) ARMAX-based transfer function model using measurement data to capture all the dominant oscillation modes. Both ambient data (by varying generation or load) and ring-down data (system large disturbances, e.g., generation trip) are used for system identification. The proposed approach is demonstrated by a case study in the 16-machine 68-bus Northeast Power Coordinating Council (NPCC) system. Results show that the identified model using ARMAX is able to accurately represent the power system dominant oscillatory behaviors. Compared with the subspace state space model, the ARMAX model has equivalent accuracy but lower order and improved computational efficiency.

The remaining content of this paper is organized as follows. Section II describes the relationship between the full-order system model and the measurement-based models. The methodology and the flowchart of system identification for oscillation damping control are presented in Section III. In Section IV, the methodology is validated by the case study in the NPCC system. Discussion and future work are given in Section V. Section VI concludes this paper.

II. Relationship Between Full-order System Model and Measurement-Based Models

The full-order system model for the small signal analysis is usually represented by the state space method which is a set of first order differential equations based on the linearization around a certain operation point, as shown in the following equations:

$$\Delta\dot{x} = A\Delta x + B\Delta u \tag{1}$$

$$\Delta y = C\Delta x + D\Delta u \tag{2}$$

where, Δx is the state vector, Δy is the output vector, and Δu is the input vector; A is the state matrix, B is the input matrix, C is the output matrix, and D is the feedforward matrix.

Obviously, the subspace state space model is indeed a kth order reduced model of the full-order system model. The only parameter that needs to be determined before A–D matrix estimation is the reduced model order, which requires SVD of a large-dimensional matrix. On the other hand, the MIMO ARMAX model is the equivalent discrete transfer function model of the original system. Based on (1) and (2), the continuous transfer function between inputs and outputs is represented as

$$G(s) = C(sI - A)^{-1}B + D. \tag{3}$$

If the inputs and outputs of the system are determined, the system model can be represented as

$$\begin{bmatrix} G_{11}(s) & \cdots & G_{1n}(s) \\ G_{21}(s) & \cdots & G_{2n}(s) \\ \vdots & \cdots & \vdots \\ G_{m1}(s) & \cdots & G_{mn}(s) \end{bmatrix} \begin{bmatrix} \Delta u_1(s) \\ \Delta u_2(s) \\ \vdots \\ \Delta u_n(s) \end{bmatrix} = \begin{bmatrix} \Delta y_1(s) \\ \Delta y_2(s) \\ \vdots \\ \Delta y_m(s) \end{bmatrix} \tag{4}$$

where $\Delta u_i(s)$ and $\Delta y_j(s)$ are the ith and jth elements of the input vector and the output vector, respectively. G_{ij} is the element of the G matrix at position (i, j). m and n are the number of system outputs and the number of system inputs, respectively.

Since the denominator of each element G_{ij} of G contains the common eigenvalues of the system [22], (3) can be expressed as

$$G(s) = \frac{1}{\prod_{i=1}^{r}(s - \lambda_i)}\bar{G}(s) \tag{5}$$

where λ_i is ith mode in the system. In the model, the characteristic polynomial has interarea modes which are observable to most of the system and local modes which are observable to the certain part of the system. The common denominator can reduce the model order substantially since the transfer function derived here is a reduced order model of the full power system model.

Equation (4) shows that the certain output may be regarded as the aggregated result from the contribution of all the inputs. Therefore, in the discrete-time domain, the contribution of the input signals to the outputs at the sampling time t can be exhibited as [9]

$$\alpha(z)y(t) = \beta(z)u(t) + \gamma(z)e(t) \tag{6}$$

where $\mathrm{y}(t)$ is the vector of m outputs, $u(t)$ is the exogenous part which is the vector containing the known p excitations, and $e(t)$ is the moving average part which is the vector with q

unknown noise. $p+q=n\cdot\alpha(z)$, $\beta(z)$ and $\gamma(z)$ are the autoregressive polynomial matrix, the exogenous polynomial matrix, and the moving average polynomial matrix, respectively. z is the shift operator

$$\alpha(z)=I+\alpha^1\times z^{-1}+\cdots+\alpha^{n_a}\times z^{-n_\alpha} \tag{7}$$

$$\beta(z)=\beta^0+\beta^1\times z^{-1}+\cdots+\beta^{n_\beta}\times z^{-n_\beta} \tag{8}$$

$$\gamma(z)=I+\gamma^1\times z^{-1}+\cdots+\gamma^{n_\gamma}\times z^{-n_\gamma}. \tag{9}$$

The matrices $\alpha(z)$, $\beta(z)$, and $\gamma(z)$ in (7)–(9) can be expanded as

$$\alpha(z)=\begin{bmatrix}1&\cdots&0\\ \vdots&\ddots&\vdots\\ 0&\cdots&1\end{bmatrix}+\begin{bmatrix}\alpha_{11}^{(1)}&\cdots&\alpha_{1m}^{(1)}\\ \vdots&\ddots&\vdots\\ \alpha_{m1}^{(1)}&\cdots&\alpha_{mm}^{(1)}\end{bmatrix}\times z^{-1}+\cdots+\begin{bmatrix}\alpha_{11}^{(n_\alpha)}&\cdots&\alpha_{1m}^{(n_\alpha)}\\ \vdots&\ddots&\vdots\\ \alpha_{m1}^{(n_\alpha)}&\cdots&\alpha_{mm}^{(n_\alpha)}\end{bmatrix}\times z^{-n_\alpha} \tag{10}$$

$$\beta(z)=\begin{bmatrix}\beta_{11}^{(0)}&\cdots&\beta_{1p}^{(0)}\\ \vdots&\ddots&\vdots\\ \beta_{m1}^{(0)}&\cdots&\beta_{mp}^{(0)}\end{bmatrix}+\begin{bmatrix}\beta_{11}^{(1)}&\cdots&\beta_{1p}^{(1)}\\ \vdots&\ddots&\vdots\\ \beta_{m1}^{(1)}&\cdots&\beta_{mp}^{(1)}\end{bmatrix}\times z^{-1}+\cdots+\begin{bmatrix}\beta_{11}^{(n_\beta)}&\cdots&\beta_{1p}^{(n_\beta)}\\ \vdots&\ddots&\vdots\\ \beta_{m1}^{(n_\beta)}&\cdots&\beta_{mp}^{(n_\beta)}\end{bmatrix}\times z^{-n_\beta} \tag{11}$$

$$\gamma(z)=\begin{bmatrix}1&\cdots&0\\ \vdots&\ddots&\vdots\\ 0&\cdots&1\end{bmatrix}+\begin{bmatrix}\gamma_{11}^{(1)}&\cdots&\gamma_{1q}^{(1)}\\ \vdots&\ddots&\vdots\\ \gamma_{m1}^{(1)}&\cdots&\gamma_{mq}^{(1)}\end{bmatrix}\times z^{-1}+\cdots+\begin{bmatrix}\gamma_{11}^{(n_\gamma)}&\cdots&\gamma_{1q}^{(n_\gamma)}\\ \vdots&\ddots&\vdots\\ \gamma_{m1}^{(n_\gamma)}&\cdots&\gamma_{mq}^{(n_\gamma)}\end{bmatrix}\times z^{-n_\gamma} \tag{12}$$

where n_α, n_β, and n_γ are the orders of the outputs, exogenous inputs, and noise, respectively. $\alpha(z)$ is an $m\times m$ matrix, $\beta(z)$ is an $m\times p$ matrix, and $\gamma(z)$ is an $m\times q$ matrix.

In order to calculate the coefficient matrix, the two-stage least square algorithm is detailed in the Appendix.

The MIMO ARMAX model is identified in the discrete-time domain. If converted into the continuous-time domain, the system transfer function can be represented by a polynomial function as

$$G(s)=y(s)\times\begin{bmatrix}u(s)\\ e(s)\end{bmatrix}^{-1}=\left[\alpha^{-1}(z)\beta(z)\alpha^{-1}(z)\gamma(z)\right]_{z=e^{sT_s}} \tag{13}$$

where T_s is the sampling period

$$G(s)=\frac{\alpha^*(z)}{|\alpha(z)|}\left[\beta(z)\gamma(z)\right]_{z=e^{sT_s}} \tag{14}$$

where $\alpha^*(z)$ is the adjugate matrix of $\alpha(z)$ and $|\alpha(z)|$ can be rewritten as

$$\prod_{i=1}^{r}(s-\lambda_i)=|\alpha(z)|_{z=e^{sT_s}}. \tag{15}$$

Since the identification procedure may introduce the unexpected modes which are numerical artifacts and weaker modes, these modes need to be filtered out from the dominant low frequency modes which range from 0.2 to 2.5 Hz. In [23], a feasible method which can finish selecting the modes through pseudo-energy from the MIMO ARMAX model has been employed in the proposed method. The modes with the highest energy may be the true system modes, and ones with low energy would be fake modes.

Based on above analysis, both MIMO subspace state space model and MIMO ARMAX model are equivalent transfer function models of the original system. The subspace state space model is represented by a set of differential equations in continuous-time domain, while the MIMO ARMAX model is represented by a set of difference equations in discrete-time domain.

III. Methodology for ARMAX Model Identification

This section introduces the methodology to build the MIMO ARMAX model using measurement data to capture dominant interarea modes of the power system for oscillation damping control. The block diagram of the presented methodology is shown in Fig. 1, which consists of five steps: 1) input selection; 2) output selection; 3) identification trigger; 4) model estimation; and 5) model validation. The adaptive and coordinated control design based on the validated MIMO ARMAX model is discussed in Section V.

A. ARMAX Model Input Selection

The first step is to choose the input signals. If applying the ARMAX model for an oscillation mode meter, any measurable signal can be selected as the input of the ARMAX model. However, since the purpose of the ARMAX model in this paper is oscillation damping control, actual controllable signals in the power system should be selected as the inputs of the ARMAX model, e.g., the controllable setpoint signals of PSS, FACTs devices, and HVDC links. In other words, the input signals of the ARMAX model can be controlled and modulated to suppress the target oscillation modes. Furthermore, in order to reduce the number of the ARMAX inputs, the conventional residue method can be used to preselect the signal with high sensitivity of dominant oscillation modes.

Taking PSS as an example, the selected input signal is illustrated in Fig. 2. The voltage reference of the excitation system (V_{ref}) is usually a given constant value to maintain the generator terminal voltage around its rating value. For a local PSS, its output (V_{pss}) is added to the V_{ref} to provide damping to suppress local oscillation modes. If using probing data for ARMAX model identification, the sum of V_{ref} and the probing signal can be selected as the input. Nevertheless, when using ambient data or ring-down data, since there is no variant signal

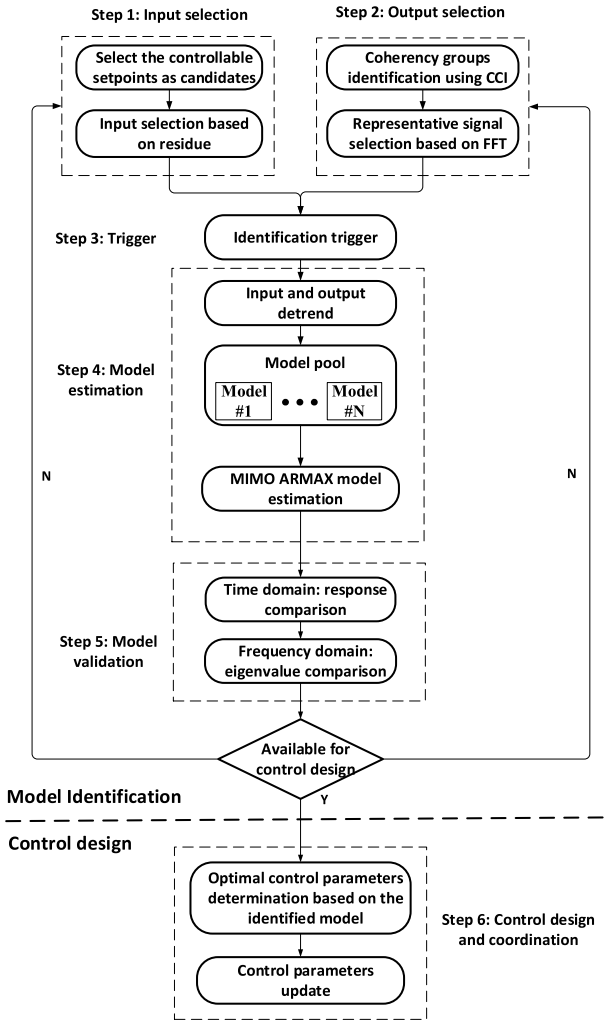

Fig. 1. Flowchart of the proposed model identification methodology.

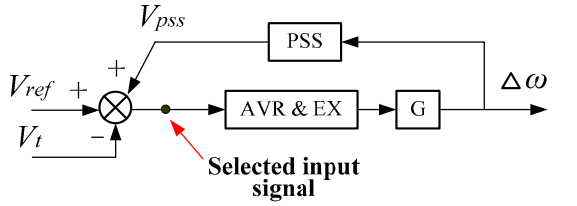

AVR: automatic voltage regulator
EX: exciter
G: generator
PSS: power system stabilizer
V_{pss}: output of PSS
V_{ref}: voltage reference
V_t: generator terminal voltage
$\Delta\omega$: rotor angular speed deviation

Fig. 2. Illustration of the input signal of the ARMAX model.

added to V_{ref}, the summation of the voltage reference, terminal voltage (V_t), and the output of PSS, is selected as the input signal of the ARMAX model.

B. ARMAX Model Output Selection

The outputs of the ARMAX model should be able to reflect the dominant modes in the power system. Rotor angular speed, tie-line active power, and generator bus frequency are the most commonly used observation signals to reflect oscillations. These types of signals can be selected as the outputs of the ARMAX model.

For a large power system, it is unnecessary to select too many signals as the outputs of the ARMAX model. Instead, it is feasible to select one representative signal for each coherent group to reduce the output number of the ARMAX model. Traditionally, coherency analysis is conducted by using a classical two-order generator model in the offline environment [24]. This paper utilizes the correlation coefficient index (CCI) [25] to identify the coherency groups online using pure measurement data in the online environment.

The process of identifying coherent machines does not necessarily guarantee that interarea modes can be observed in the measurements. Therefore, the fast Fourier transform (FFT) algorithm is adopted to select the optimal output of the ARMAX model in each coherent group after the coherency analysis. The candidate measurement signals are ranked from high to low according to the normalized magnitude at the frequency point of the dominant modes, and then the highest one in each coherent group will be selected as the outputs of the ARMAX model. Summarily, the criterion for the representative outputs in each of coherency groups is that they have the best observability for all target interarea oscillation modes through the FFT computation. Furthermore, In order to retain the characteristics for the full system, each coherency group may keep a measurement at least.

C. Identification Trigger

Three types of measurement data (probing data, ambient data, and ring-down data) can be utilized to build the ARMAX model [26]–[28]. For a large power grid, probing data are theoretically ideal to build the model because system response usually contains most of the modes when a probing signal is injected into the system. However, probing data require consistent excitations, which is not practical during system operation. Compared with probing data, ambient data, and ring-down data are much easier to be collected in the online environment because they can be measured when load variation/generation regulation is within a small range or with large system disturbances (e.g., line trips, generation trips, and load sheddings) during system operation. Hence, both ambient data and ring-down data are considered in this paper.

The online model identification is triggered by system events including generation trips, load sheddings, and topology changes due to line trips, etc., these system events can be detected by the existing situational awareness functions based on wide-area measurement. If there are events, the model will be update immediately when the data collection is ready. In addition, the identification procedure can be triggered by predefined timer (periodical trigger). If there is no system events, the model will be updated using collected ambient data in every 5 min.

D. ARMAX Model Estimation

Before using the ambient data and ring-down data, it is necessary to remove direct current trends within the measurement data. Normally, this operation is known as de-trending,

and keeps the result from being overwhelmed by the nonzero mean and the trend terms.

There are several candidate models in the model pool, which is expected to avoid revising models several times in one update cycle so that the identification process can keep the computational efficiency. In the model pool, the orders of the MIMO ARMAX models have been adopted depending on the priori knowledge. The highest order of the MIMO ARMAX model in the model pool is 50. When the identification is triggered, these ARMAX models with different orders in the model pool will be identified simultaneously. The model coefficients in (10)–(12) can be computed by using the two-stage least square algorithm as shown in the Appendix. The model with highest accuracy indices in both time domain and frequency domain specified in the next section is selected as the identified model. If the identification results from all MIMO ARMAX models cannot fulfill the accuracy requirements, the current identification would be abandoned. The parameters of the adaptive controllers would not be model updated in this cycle.

E. ARMAX Model Validation

After identifying the ARMAX model, it is necessary to validate whether the model is good enough to describe the system oscillatory characteristics. The identified ARMAX model is validated in both time domain and frequency domain.

In time domain, the response of the identified model is compared with actual response. In order to determine if the response of the model matches with the actual one, the fitting accuracy index is defined as

$$\text{Accuracy Index} = \left(1 - \frac{\left\|Y_i - \hat{Y}_i\right\|}{\left\|Y_i - \bar{Y}_i\right\|}\right) \times 100\% \qquad (16)$$

where Y_i is the response of the constructed model, $\hat{Y}_i$ is the response of the actual system, and $\bar{Y}_i$ is the mean of actual system response over several periods. If this index is closer to 100%, it indicates that the response of the model under validation matches the actual system better.

In frequency domain, the eigenvalues calculated by the denominator polynomial of the MIMO ARMAX model are compared with results of matrix pencil (MP) analysis of the measurement data. MP is a modal extraction technique (similar to Prony method), which effectively estimates the dominant modes' information in a response [29]. In (15), the modes of the system can be derived from the denominator of the polynomial function. Based on the sampling period T_s, a mode with real part σ and imaginary part ω can be written as

$$\sigma + j\omega = \frac{1}{T_s} \times \ln(\xi) \qquad (17)$$

where ξ is a vector of poles in the z-domain.

The criterion, which determines the model is good or not, is that the accuracy index is over 85%, and the deviations of real parts and imaginary parts of eigenvalues in frequency domain are less than 0.05, compared with the results of MP.

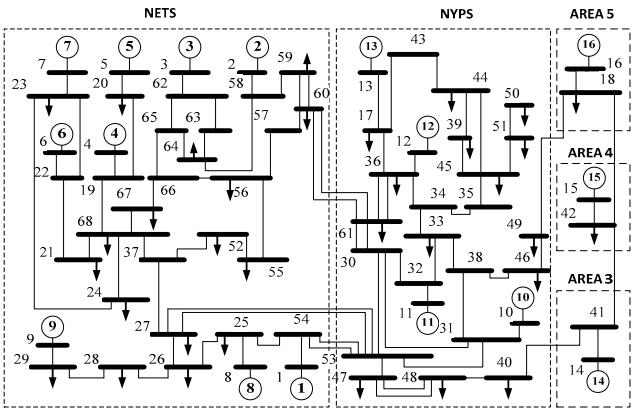

Fig. 3. Single line diagram of the 16-machine 68-bus NPCC system.

TABLE I
MODAL ANALYSIS OF THE NPCC SYSTEM

	Type	Frequency (Hz)	Damping ratio(%)	Participated generators
1	Inter-area	0.38	15.90	G1~G13 vs. G14, G15
2	Inter-area	0.41	6.38	G1~G14 vs. G15, G16
3	Inter-area	0.63	3.57	G1~G9 vs. G10~G13
4	Inter-area	0.83	5.28	G14, G16 vs. G15

Supposing the inputs and outputs are temporarily unavailable due to the topology changes, the selection of inputs and outputs needs to be redone manually.

IV. CASE STUDY

A. Brief Introduction of the NPCC System

The proposed method is validated in the 16-machine 68-bus NPCC system, which is a reduced order model of the New England test system (NETS)/New York power system (NYPS) interconnected system. As shown in Fig. 3, NETS and NYPS are represented by two groups of generators (G1 to G9, and G10 to G13), respectively. Three other neighboring areas are approximated by equivalent generator models (G14 to G16). Generators G1 to G8 and G10 to G13 have direct current excitation systems, while G9 has fast static excitation. The rest of the generators have manual excitation. In order to create multiple oscillation modes with poor damping ratios, only G1 to G3, and G8 to G9 are equipped with local PSSs. The system parameters can be referred to [30].

The study system has four dominant interarea oscillation modes. Their oscillation frequencies and damping ratios are given in Table I. There are three modes with poor damping ratio. It is noted that the 0.63 Hz mode has the smallest damping ratio, in which the generators in NETS oscillate against the generators in NYPS.

It is assumed that PMU devices are installed at all the buses to measure bus frequency and generator variables, like voltage reference of excitation system, PSS output, and generator terminal voltage. In this paper, measurement data are generated by dynamic simulation in MATLAB/Simulink. According to the PMU measurement accuracy specified in the standard IEEE C37.118-1, a randomized time-variant measurement

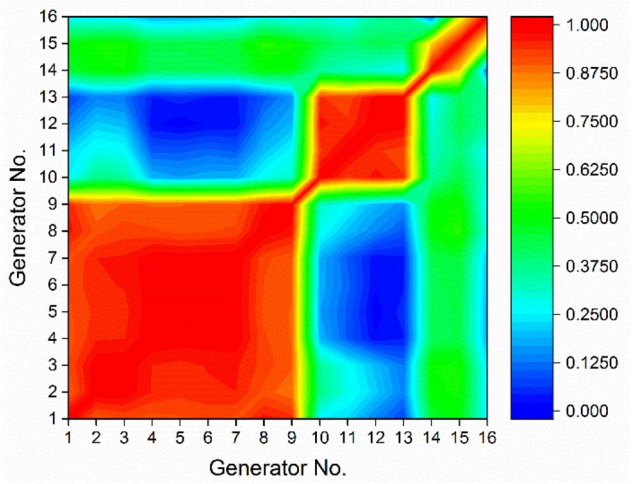

Fig. 4. Coherency analysis based on CCI.

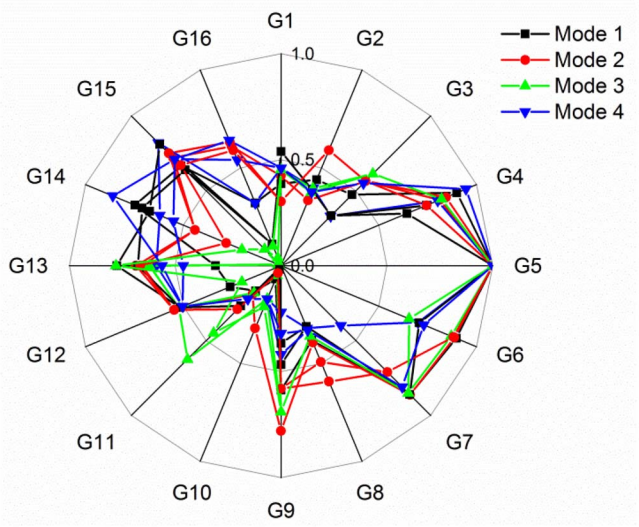

Fig. 5. Observation signal selection results using FFT analysis of three tests.

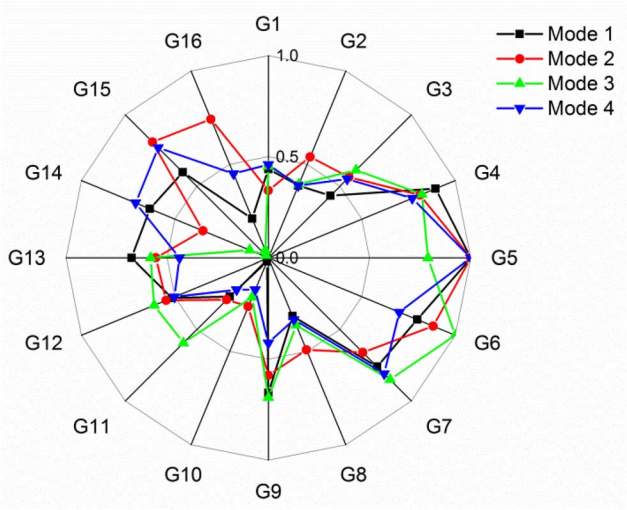

Fig. 6. Observation signal selection results using residue method.

error within 5mHz is added to the simulation data [31]. The simulation data and the measurement error together are considered to be real-measurement data collected by field PMUs.

B. Input and Output Selection

As mentioned in Section III-A, the controllable setpoint signals of a power system should be selected as the input signals. Since there are five generators equipped with local PSSs, and ambient data and ring-down data are utilized for model identification, the sum of voltage reference, terminal voltage, and output of PSS at each of these five generators is selected as an input signal of the ARMAX model.

The output selection is based on coherency analysis and FFT analysis. The results of CCI-based coherency analysis are given in Fig. 4. The red part, green part, and blue part represent high, intermediate, and low coherency between different generators, respectively. The results illustrate that the study system can be divided into five coherency groups: 1) G1 to G9; 2) G10 to G13; 3) G14; 4) G15; and 5) G16. The coherency analysis results are consistent with those of the conventional method [22]. In this paper, frequency signals at each generator bus are the candidate output signals. Since G14–G16 are the equivalent generators in coherency groups 3–5, respectively, bus frequency f14–f16 are selected as the representative signal of each coherency groups.

In order to select one representative signal for groups 1 and 2, all the generator bus frequency signals in groups 1 and 2 are analyzed by using FFT analysis in several separate tests. The normalized results of FFT analysis are shown in the radar chart in Fig. 5. Bus frequency at buses 5 and 13 always have the highest amplitudes for four dominant interarea modes under these different operating conditions. The above result can be compared and verified by the results derived from the residue method based on the full-order system model. Fig. 6 shows the magnitude of different generator buses in the residue analysis. Thus, the analysis result based on measurement match with the result from the circuit model. Finally, bus frequencies f5, f13–f16 are the selected observation signals for coherency groups 1–5, respectively.

C. Performance of the MIMO ARMAX Model

Both ambient data and ring-down data are applied to build the MIMO ARMAX model. As mentioned in Section III-D, the fitting accuracy index is used for time domain validation, while the results from the MP algorithm are selected as the benchmark in frequency domain validation. Additionally, the MIMO ARMAX model is compared with the MIMO N4SID model in estimation accuracy and computation time. Base on numerous offline experiments, the structures of models in the model pool can be determined. The best four different orders of the MIMO ARMAX models for identification using ambient data and ring-down data are (6, 4, 3), (8, 5, 3), (12, 8, 5), and (15, 9, 5), while the best four different orders of the MIMO N4SID models are 30, 40, 50, and 60.

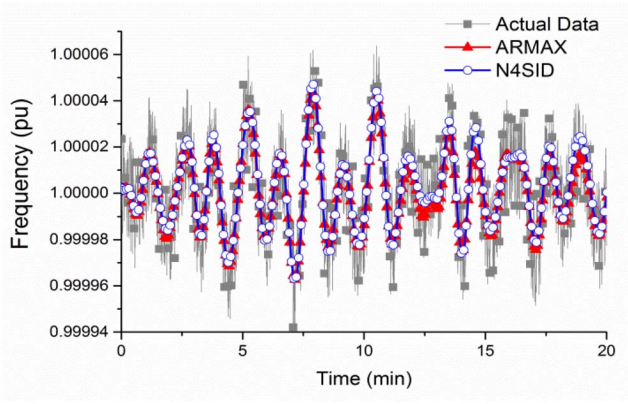

Fig. 7. Comparison of bus frequency response at bus 5 (generation modulation at bus 3).

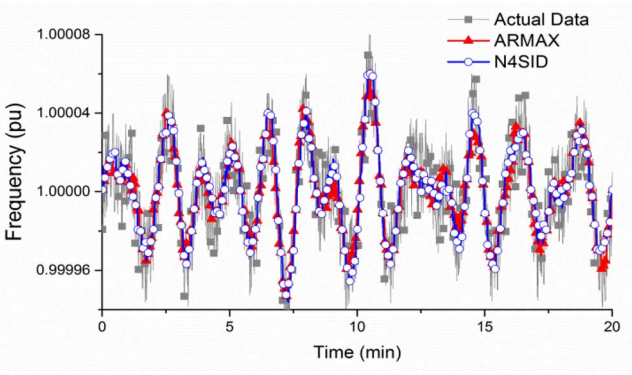

Fig. 8. Comparison of bus frequency response at bus 5 (load modulation at bus 10).

1) Ambient Data: The ambient data are created by modulating generation (or load) within a narrow range (±2%) at each generator bus (or load bus). These 50 (16 generator buses and 34 load buses) independent sets of ambient data are used to build the MIMO ARMAX model and the MIMO N4SID model. In addition, the measurement error within 5mHz is injected into the output signals to emulate the noise in the measurement data. The data is downsampled to a rate of 5 samples per second and 5 min window size length is chosen in the ambient data analysis.

Taking the independent sets of ambient data by generation modulation at bus 3 and load modulation at bus 10 for instance, Figs. 7 and 8 show the time domain response comparison of the actual system, the MIMO ARMAX model and the MIMO N4SID model in these two cases, respectively. The optimal order of the MIMO ARMAX model for maximum fitting accuracy is $(n_\alpha, n_\beta, n_\gamma) = (8, 5, 3)$, while the optimal order of the MIMO N4SID model is 40. Both MIMO ARMAX model and MIMO N4SID model have similar time domain response with the actual system even if measurement error is present. Due to page limitation, other four outputs of the measurement-based models (frequency of buses 13–16) are not given (similarly hereinafter).

In frequency domain, the eigenvalues of all of the four dominant interarea modes are also estimated by using the MP algorithm, the MIMO ARMAX model, and the MIMO N4SID model using the 50 independent sets of ambient data. For the optimal orders in two models, the eigenvalues comparison and the error of modes identification comparing with MP are shown in Fig. 9 and Table II which contains absolute values of maximum bias (Max.) and standard deviation (Std.), respectively. Both MIMO ARMAX model and MIMO N4SID model can capture all the interarea oscillation modes. Nevertheless, the estimation results of the MIMO ARMAX model are slightly closer to the benchmark than the MIMO N4SID model.

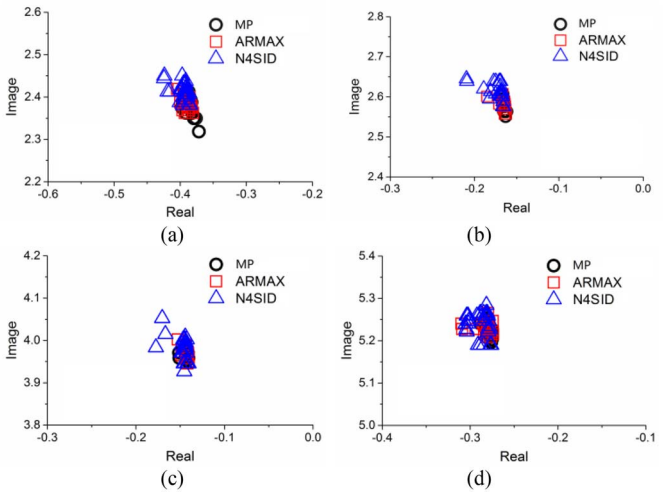

Fig. 9. Eigenvalue comparison. (a) Model 1 (0.38 Hz). (b) Mode 2 (0.41 Hz). (c) Mode 3 (0.63 Hz). (d) Mode 4 (0.83 Hz).

TABLE II
ACCURACY OF MODES FOR ARMAX AND N4SID USING AMBIENT DATA

		Bias	Mode1	Mode2	Mode3	Mode4
MIMO ARMAX	Real	Max.	0.04	0.03	0.02	0.05
		Std.	0.01	0.02	0.01	0.01
	Imag.	Max.	0.05	0.03	0.03	0.02
		Std.	0.00	0.01	0.02	0.01
MIMO N4SID	Real	Max.	0.08	0.07	0.05	0.08
		Std.	0.02	0.02	0.03	0.04
	Imag.	Max.	0.10	0.11	0.14	0.05
		Std.	0.02	0.01	0.05	0.02

2) Ring-down Data: Generation trip, load shedding, and line trip events are generated to demonstrate how the proposed methodology behaves with the ring-down data. The sampling rate is 30 samples per second, and the data window is 10 s. In order to eliminate the impact of system transient, the first swing data is removed for model identification. Also, 5 mHz measurement error is included.

Figs. 10 and 11 are two cases of validation using the 53 (16 generations, 34 loads, and 3 tie-lines) independent sets of ring-down data. Fig. 10 shows the bus frequency response at bus 5 in case of 20% generation trip of G3 at time $t = 1$ s. Fig. 11 shows the bus frequency response at bus 5 in case of 20% load shedding at bus 39 at time $t = 1$ s. In the two cases, the optimal order the MIMO ARMAX model is $(n_\alpha, n_\beta, n_\gamma) = (12, 8, 5)$, and the optimal order the MIMO N4SID model is 60.

For the optimal orders in two models from all sets of ring-down data, the comparison of the estimated eigenvalues

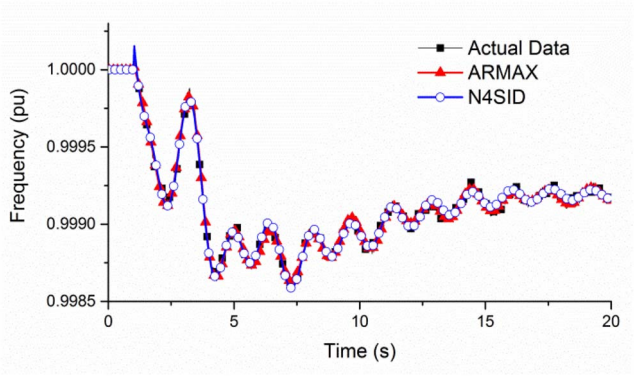

Fig. 10. Comparison of bus frequency response at bus 5 (20% generation trip of G3).

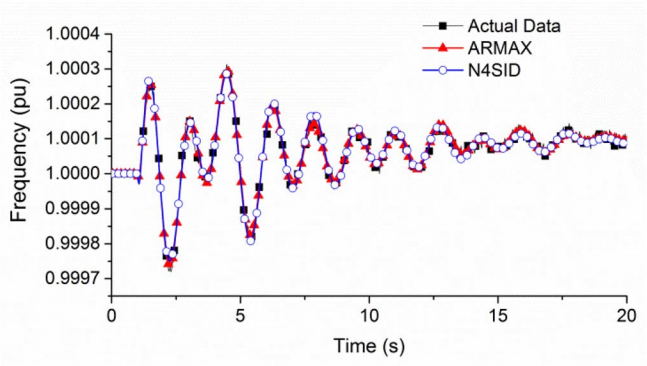

Fig. 11. Comparison of bus frequency response at bus 5 (20% load shedding at bus 39).

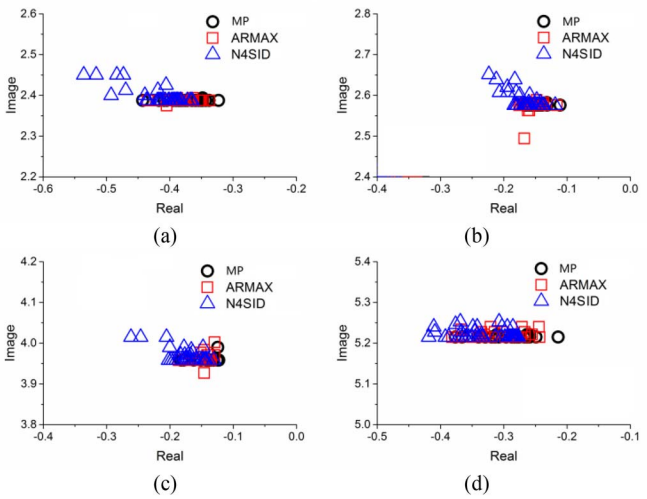

Fig. 12. Eigenvalue comparison. (a) Model 1 (0.38 Hz). (b) Mode 2 (0.41 Hz). (c) Mode 3 (0.63 Hz). (d) Mode 4 (0.83 Hz).

using each independent set of ring-down data and the error of modes identification comparing with MP are given in Fig. 12 and Table III, which contains absolute values of maximum bias (Max.) and standard deviation (Std.), respectively.

Similarly, both MIMO ARMAX model and MIMO N4SID model can capture all the dominant oscillation modes of the study system. The event data at the first swing are removed

TABLE III
ACCURACY OF MODES FOR ARMAX AND N4SID USING RINGDOWN DATA

		Bias	Mode1	Mode2	Mode3	Mode4
MIMO ARMAX	Real	Max.	0.11	0.05	0.05	0.10
		Std.	0.02	0.01	0.02	0.03
	Imag.	Max.	0.03	0.07	0.05	0.04
		Std.	0.02	0.01	0.01	0.02
MIMO N4SID	Real	Max.	0.20	0.10	0.13	0.10
		Std.	0.05	0.04	0.06	0.09
	Imag.	Max.	0.10	0.07	0.07	0.05
		Std.	0.03	0.02	0.03	0.03

TABLE IV
PERFORMANCE COMPARISON OF THE TWO MODELS IN MODEL POOL

Data type	Model type	Model order	Accuracy Index (%)	Time (sec)
Ambient	ARMAX	(6, 4, 3)	81.2	0.85
	ARMAX	(8, 5, 3)	91.4	0.93
	ARMAX	(12, 8, 5)	86.1	1.14
	ARMAX	(15, 9, 5)	82.5	2.17
	N4SID	30	78.2	6.40
	N4SID	40	86.5	7.71
	N4SID	50	84.3	8.23
	N4SID	60	74.7	8.44
Ring-down	ARMAX	(6, 4, 3)	78.1	0.88
	ARMAX	(8, 5, 3)	83.6	1.02
	ARMAX	(12, 8, 5)	91.8	1.26
	ARMAX	(15, 9, 5)	89.2	2.10
	N4SID	30	61.7	4.67
	N4SID	40	65.3	6.27
	N4SID	50	74.1	7.35
	N4SID	60	85.4	8.61

for the identification since the strong nonlinearity may corrupt the model identification.

The estimation accuracy and computation time comparison of the two models are shown in Table IV. The cases "generation modulation at bus 3" and "20% load shedding at bus 39" are selected as examples. In order to have equivalent fitting accuracy and mode estimation results with the MIMO ARMAX model, it is necessary to increase the order of the MIMO N4SID model. For instance, when using ring-down data, the MIMO N4SID models with low order are not capable of exhibiting the dynamic behavior under the contingencies in the system unless the order is increased to 60. If the order of the MIMO N4SID model is 40 (or 50), the fitting accuracy index is 65.3% (or 74.1%). However, the order of the MIMO ARMAX model is $(n_\alpha, n_\beta, n_\gamma) = (12, 8, 5)$, which is much less.

More importantly, if two models needs to get similar result, the MIMO N4SID model identification requires about 7–8 s, while the MIMO ARMAX model requires about 1 s. The computation time of the MIMO ARMAX model is much less than the MIMO N4SID model. It is noted that although the order of the MIMO ARMAX for identifying the ring-down data is higher than the order for identifying the ambient data, the computational speed does not increase significantly.

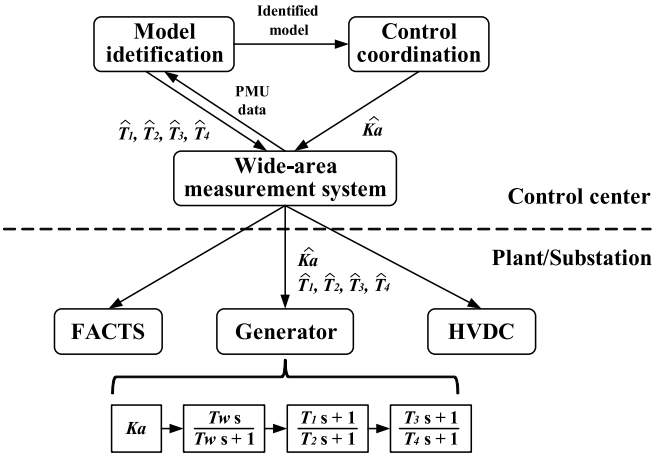

Fig. 13. General architecture of the adaptive and coordinated oscillation damping control system.

V. Discussion and Future Work

The use of the MIMO ARMAX model has many obvious and potential benefits. The simplest but most important one is that the model is a measurement-based model, which requires very little prior information about the system. Since the MIMO ARMAX model selects actual controllable signals in a power system as the inputs, it is a causal model which is able to capture all the dominant oscillation modes and represent the entire power system for oscillation damping control. More importantly, the MIMO ARMAX model has equivalent accuracy with the MIMO subspace state space model, but requires lower order and less computation time. Hence, it is more suitable to improve adaptivity and coordination of the oscillation damping control system in the online environment. Moreover, the case study shows the circumstance where only the setpoints of PSS are selected as the input of the ARMAX model. If FACTS devices and HVDC links are employed by power system, the proposed methodology still applies for the circumstances where the setpoints of FACTS devices and HVDC links are selecting as the inputs signals.

The general architecture of the adaptive and coordinated oscillation damping control system is shown in Fig. 13. Taking one wide-area oscillation damping controller at a generation based on lead-lag compensation for instance, the MIMO ARMAX model is identified using ambient data or ring-down data from WAMS. In normal operating conditions, the model will be updated using ambient data. The model updating rate could be once per 5 min. If an event (e.g., line trip, generation trip, or load shedding) occurs, the model is updated using the latest ring-down data. The model could be updated within 11–12 s (including data window and computation time). The starting point of the ring-down data can be determined by event detection function in WAMS. It is noted that the identified model is a closed-loop system model, which includes the controller requiring parameter update. However, since the parameters of the controller are already known, it is not difficult to derive the open-loop system model which excludes the controller.

Based on the identified model, the residue phase can be estimated under the latest operating condition, and is used to update the parameters of the lead-lag compensator (T_1–T_4). Moreover, the optimal gain (Ka) is determined by optimization to maximize the overall damping improvement of all oscillation modes in consideration. The updated control parameters are remotely configured to dispersed controllers in different power plants and substations.

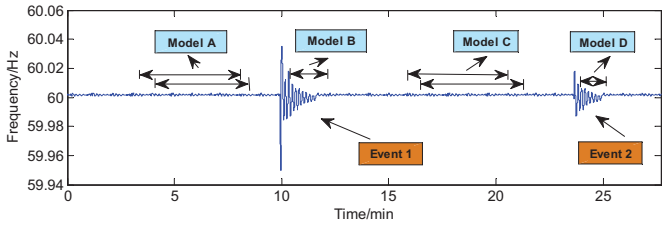

Fig. 14. Time sequence of the adaptive approach.

Fig. 14 shows the time sequence of the adaptive approach. Model A is identified using the ambient data, and then the oscillation damping controllers are tuned based on Mode A for the next disturbance. If there is no event, Model A and controller parameters are updated using the ambient data in the next data window. When an event (Event 1) occurs, the controllers will perform with tuned parameters based on the latest Model A. After Event 1 occurred, Model B is identified using the ring-down data, and the controller parameters can be updated based on Model B. Although the controllers perform with the parameters tuned based on Model A (not Model B) during Event 1, the oscillation damping control system is able to track the continuous variation of operating conditions and ready to experience the next disturbance. Similarly, Model C can be identified by the ambient data after Event 1, while Model D will be identified using the ring-down data in Event 2 to tune controllers for the subsequent disturbance.

Our future work will focus on application of the MIMO ARMAX model into adaptive and coordinated oscillation damping control, including control architecture, coordinated control scheme, remote parameter configuration, and demonstration in hardware test-bed.

VI. Conclusion

Aiming for the adaptive and coordinated oscillation damping control, the methodology to identify the MIMO ARMAX-based transfer function model using pure measurement is proposed in this paper. The case study in the NPCC system demonstrates that the identified MIMO ARMAX model using ambient data or ring-down data is able to accurately capture all the dominant oscillation modes.

The time domain response of the MIMO ARMAX model reflects that of the actual system, and the estimated eigenvalues are very close to the results of MP analysis. Compared with the MIMO subspace state model, the MIMO ARMAX model has equivalent accuracy but lower order and less computation time. Future work will focus on applying the MIMO ARMAX model for adaptive and coordinated oscillation damping control.

APPENDIX

The two-stage least square approach is provided in [9] for the SISO ARMAX algorithm, and is extended to the MIMO ARMAX case in (6). The least square algorithm may be applied twice in two stages. The first stage is to estimate the unknown random inputs for the MIMO ARMAX model through the MIMO ARX model

$$\alpha^F(z)y(t) = \beta^F(z)u(t) + e(t) \tag{A1}$$

where F is the order of autoregressive and input parts of the model, and F is higher than any of the orders in the MIMO ARMAX model but is not more than double of the highest order in the MIMO ARMAX.

The linear regression vector in [9] can be presented as

$$\begin{aligned}\varphi^F(t) = \big[&-y^T(t-1)\cdots - y^T(t-F)\\ &u^T(t-1)\cdots u^T(t-F)\big]^T\end{aligned} \tag{A2}$$

and $\Theta^F$is the coefficient matrix

$$\Theta^F = \begin{bmatrix}\alpha_1^F \cdots \alpha_F^F & \beta_1^F \cdots \beta_F^F\end{bmatrix}^T \tag{A3}$$

where α_i^F is ith autoregressive coefficient matrix, and β_i^F is ith known input matrix. The first least square estimation from N samples of measurement is

$$\hat{\Theta}^F = \left[\frac{1}{N}\sum_{t=1}^{N}\varphi^F(t)\big[\varphi^F(t)\big]^T\right]^{-1}\left[\frac{1}{N}\sum_{t=1}^{N}\varphi^F(t)y^T(t)\right]. \tag{A4}$$

The estimated unknown inputs are

$$\hat{e}(t) = \hat{\alpha}^F(z)y(t) - \hat{\beta}^F(z)u(t). \tag{A5}$$

Therefore, (6) can be modified as (A6), which is the pseudo-ARMAX model since it contains the estimation results

$$\alpha(z)y(t) = \beta(z)u(t) + \gamma(z)\hat{e}(t). \tag{A6}$$

Similarly, the linear regression is pseudo-linear regress

$$\begin{aligned}\hat{\varphi}(t) = \big[&-y^T(t-1)\cdots - y^T(t-n_a)\\ &u^T(t-1)\cdots u^T(t-n_b)^T\\ &\hat{e}^T(t-1)\cdots \hat{e}^T(t-n_c)\big].\end{aligned} \tag{A7}$$

Thus, the coefficient matrix is

$$\Theta = \begin{bmatrix}\alpha^1 \cdots \alpha^{n_a} & \beta^1 \cdots \beta^{n_b} & \gamma^1 \cdots \gamma^{n_c}\end{bmatrix}^T. \tag{A8}$$

The estimated coefficients of the MIMO ARMAX model can be obtained from the second stage of the least square algorithm

$$\hat{\Theta} = \left[\frac{1}{N}\sum_{t=1}^{N}\hat{\varphi}(t)\hat{\varphi}^T(t)\right]^{-1}\left[\frac{1}{N}\sum_{t=1}^{N}\hat{\varphi}(t)y^T(t)\right] \tag{A9}$$

where $\hat{\Theta}$ is the matrix coefficients which can be calculated by two-stage least square.

REFERENCES

[1] B. Pal and B. Chaudhuri, *Robust Control in Power Systems*. New York, NY, USA: Springer, 2005.

[2] M. E. About-Ela, A. A. Salam, J. D. McCalley, and A. A. Fouad, "Damping controller design for power system oscillations using global signals," *IEEE Trans. Power Syst.*, vol. 11, no. 2, pp. 767–773, May 1996.

[3] W. Yao, L. Jiang, J. Wen, Q. H. Wu, and S. Chen, "Wide-area damping controller of FACTS devices for inter-area oscillations considering communication time delay," *IEEE Trans. Power Syst.*, vol. 29, no. 1, pp. 318–329, Jan. 2014.

[4] A. Fuchs, M. Imhof, T. Demiray, and M. Morari, "Stabilization of large power systems using VSC-HVDC and model predictive control," *IEEE Trans. Power Del.*, vol. 29, no. 1, pp. 480–488, Feb. 2014.

[5] C. Zhu, M. Khammash, V. Vittal, and W. Qiu, "Robust power system stabilizer design using H_8 loop shaping approach," *IEEE Trans. Power Syst.*, vol. 18, no. 2, pp. 810–818, May 2003.

[6] R. Majumder, B. C. Pal, C. Dufour, and P. Korba, "Design and real-time implementation of robust FACTS controller for damping inter-area oscillation," *IEEE Trans. Power Syst.*, vol. 21, no. 2, pp. 809–816, May 2006.

[7] (Aug. 31, 2015). *March 2015 PMU Locations - Map of PMUs in North America*. [Online]. Available: https://www.naspi.org/documents

[8] Y. Zhang *et al.*, "Wide-area frequency monitoring network (FNET) architecture and applications," *IEEE Trans. Smart Grid*, vol. 1, no. 2, pp. 159–167, Sep. 2010.

[9] L. Ljung, *System Identification: Theory for the User*, 2nd ed. Englewood Cliffs, NJ, USA: Prentice-Hall, 1999.

[10] D. K. Chaturvedi and O. P. Malik, "Generalized neuron-based adaptive PSS for multimachine environment," *IEEE Trans. Power Syst.*, vol. 20, no. 1, pp. 358–366, Feb. 2005.

[11] J. Zhang, C. Y. Chung, C. Lu, K. Men, and L. Tu, "A novel adaptive wide area PSS based on output-only modal analysis," *IEEE Trans. Power Syst.*, vol. 30, no. 5, pp. 2633–2642, Sep. 2015.

[12] I. Kamwa, R. Grondin, and Y. Hebert, "Wide-area measurement based stabilizing control of large power systems—A decentralized/hierarchical approach," *IEEE Trans. Power Syst.*, vol. 16, no. 1, pp. 136–153, Feb. 2001.

[13] R. Eriksson and L. Söder, "Wide-area measurement system-based subspace identification for obtaining linear models to centrally coordinate controllable devices," *IEEE Trans. Power Del.*, vol. 26, no. 2, pp. 988–997, Apr. 2011.

[14] I. Kamwa and L. Gerin-Lajoie, "State-space system identification-toward MIMO models for modal analysis and optimization of bulk power systems," *IEEE Trans. Power Syst.*, vol. 15, no. 1, pp. 326–335, Feb. 2000.

[15] N. Zhou, J. W. Pierre, and J. F. Hauer, "Initial results in power system identification from injected probing signals using a subspace method," *IEEE Trans. Power Syst.*, vol. 21, no. 3, pp. 1296–1302, Aug. 2006.

[16] H. Ghasemi, C. Canizares, and A. Moshref, "Oscillatory stability limit prediction using stochastic subspace identification," *IEEE Trans. Power Syst.*, vol. 21, no. 2, pp. 736–745, May 2006.

[17] S. A. N. Sarmadi and V. Venkatasubramanian, "Electromechanical mode estimation using recursive adaptive stochastic subspace identification," *IEEE Trans. Power Syst.*, vol. 29, no 1, pp. 349–358, Jan. 2014.

[18] R. W. Wies, J. W. Pierre, and D. J. Trudnowski, "Use of ARMA block processing for estimating stationary low-frequency electromechanical modes of power systems," *IEEE Trans. Power Syst.*, vol. 18, no. 1, pp. 167–173, Feb. 2003.

[19] L. Dosiek and J. W. Pierre, "Estimating electromechanical modes and mode shapes using the multichannel ARMAX model," *IEEE Trans. Power Syst.*, vol. 28, no. 2, pp. 1950–1959, May 2013.

[20] N. R. Chaudhuri *et al.*, "Wide-area power oscillation damping control in Nordic equivalent system," *IET Gener. Transm. Distrib.*, vol. 4, no. 10, pp. 1139–1150, Oct. 2010.

[21] W. Yao, L. Jiang, J. Wen, Q. Wu, and S. Cheng, "Wide-area damping controller for power system interarea oscillations: A networked predictive control approach," *IEEE Trans. Control Syst. Technol.*, vol. 23, no. 1, pp. 27–36, Jan. 2015.

[22] N. Zhou, Z. Huang, L. Dosiek, D. Trudnowski, and J. W. Pierre, "Electromechanical mode shape estimation based on transfer function identification using PMU measurements," in *Proc. IEEE Power Energy Soc. Gen. Meeting*, Calgary, AB, Canada, 2009, pp. 1–7.

[23] D. J. Trudnowski, J. W. Pierre, N. Zhou, J. F. Hauer, and M. Parashar, "Performance of three mode-meter block-processing algorithms for automated dynamic stability assessment," *IEEE Trans. Power Syst.*, vol. 23, no. 2, pp. 680–690, May 2008.
[24] G. Rogers, *Power System Oscillations*. Boston, MA, USA: Kluwer Academic, 2000.
[25] F. Bai *et al.*, "Input signals selection for measurement-based power system ARX dynamic model response estimation," in *Proc. IEEE PES T&D Conf. Expo.*, Chicago, IL, USA, Apr. 2014, pp. 1–7.
[26] J. Turunen *et al.*, "Comparison of three electromechanical oscillation damping estimation methods," *IEEE Trans. Power Syst.*, vol. 26, no. 4, pp. 2398–2407, Nov. 2011.
[27] L. Dosiek, N. Zhou, J. W. Pierre, Z. Huang, and D. J. Trudnowski, "Mode shape estimation algorithms under ambient conditions: A comparative review," *IEEE Trans. Power Syst.*, vol. 28, no. 2, pp. 779–787, May 2013.
[28] Z. Tashman, H. Khalilinia, and V. Venkatasubramanian, "Multi-dimensional Fourier ringdown analysis for power systems using synchrophasors," *IEEE Trans. Power Syst.*, vol. 29, no. 2, pp. 731–741, Mar. 2014.
[29] M. L. Crow and A. Singh, "The matrix pencil for power system modal extraction," *IEEE Trans. Power Syst.*, vol. 20, no. 1, pp. 501–502, Feb. 2005.
[30] A. K. Singh and B. C. Pal. (Dec. 3, 2013). *IEEE PES Task Force on Benchmark System for Stability Controls Report on the 68-Bus, 16-Machine, 5-Area System.* Version 3.3. [Online]. Available: http://www.sel.eesc.usp.br/ieee/
[31] *IEEE Standard for Synchrophasor Data Transfer for Power Systems*, IEEE Standard C37.118.1, Dec. 2011.

Hesen Liu received the B.S. degree in electrical engineering from North China Electric Power University, Beijing, China, in 2005. He is currently pursuing the Ph.D. degree in electrical engineering with the Department of Electrical Engineering and Computer Science, University of Tennessee, Knoxville, TN, USA.

He was with Yunnan Power Grid Company, Kunming, China, from 2005 to 2011. His current research interests include wide-area power system measurement, and power system dynamics and control.

Lin Zhu (S'07–M'11) was born in Anhui, China, in 1982. He received the B.S. and Ph.D. degrees in electrical engineering from the Huazhong University of Science and Technology (HUST), Wuhan, China, in 2005 and 2011, respectively.

He was a Postdoctoral Research Fellow with the Department of Control Science and Engineering, HUST. He is currently a Postdoctoral Research Fellow with the Department of Electrical Engineering and Computer Science, University of Tennessee, Knoxville, TN, USA. His current research interests include protective relaying, substation automation, and power system dynamics and control.

Zhuohong Pan (M'14) was born in Canton, China, in 1982. He received the B.Sc. and Ph.D. degrees in electrical engineering from the School of Electrical Engineering, Wuhan University, Wuhan, China, in 2005 and 2011, respectively.

He is with the Department of Electrical Engineering, Wuhan University. He is currently a Visiting Scholar with the University of Tennessee, Knoxville, TN, USA. His current research interests include the study of grounding technology, electromagnetic theory, and numerical analysis.

Feifei Bai received the Ph.D. degree in electrical engineering with the Department of Electrical Engineering, Southwest Jiaotong University, Chengdu, China, in 2015.

From 2012 to 2014, she was a joint Ph.D. student with the Department of Electrical Engineering and Computer Science, University of Tennessee, Knoxville, TN, USA. Her current research interests include power system dynamics estimation, measurement-based power system low-frequency damping control, and on-line identification of coherency generator.

Yong Liu (S'11–M'13) received the B.S. and M.S. degrees from Shandong University, Jinan, China, in 2007 and 2010, respectively, and the Ph.D. degree from the University of Tennessee, Knoxville, TN, USA, in 2013, all in electrical engineering.

He is currently a Research Assistant Professor with the University of Tennessee. His current research interests include power system wide-area measurement and large-scale power system simulation.

Yilu Liu (S'88–M'89–SM'99–F'04) received the B.S. degree in electrical engineering from Xi'an Jiaotong University, Xi'an, China, and the M.S. and Ph.D. degrees in electrical engineering from Ohio State University, Columbus, OH, USA, in 1986 and 1989, respectively.

She was a Professor with Virginia Tech, Blacksburg, VA, USA. She is currently the Governor's Chair with the University of Tennessee (UTK), Knoxville, TN, USA, and Oak Ridge National Laboratory (ORNL), Oak Ridge, TN. She is also the Deputy Director of the Department of Energy/National Science Foundation cofunded Engineering Research Center CURENT, Knoxville. She led the effort to create the North American Power Grid Frequency Monitoring Network with Virginia Tech, which is currently operated at UTK and ORNL as GridEye. Her current research interests include power system wide-area monitoring and control, large interconnection-level dynamic simulations, electromagnetic transient analysis, and power transformer modeling and diagnosis.

Mahendra Patel (M'74–SM'81) received the B.S. degree in electrical engineering from Sardar Patel University, Vallabh Vidhyanagar, India, in 1971; the M.S.E.E. degree in electrical engineering from West Virginia University, Morgantown, WV, USA, in 1979; and the M.B.A. degree in business administration from the University of Pittsburgh, Pittsburgh, PA, USA, in 1983.

He has researched in electric power utilities for over 32 years, mainly in the areas of system dynamics, voltage stability, and network transient analysis. He joined PJM, Audubon, PA, USA, in 2002, where he was a Manager of Generation Analysis, responsible for system dynamics analysis and generation and merchant transmission interconnection planning. He is currently a Senior Project Engineer/Scientist with the Electric Power Research Institute, Palo Alto, CA, USA.

Evangelos Farantatos (S'06–M'13) was born in Athens, Greece, in 1983. He received the Diploma degree in electrical and computer engineering from the National Technical University of Athens, Athens, in 2006, and the M.S. degree in electronics and communication engineering, and the Ph.D. degree in electrical engineering from the Georgia Institute of Technology, Atlanta, GA, USA, in 2009 and 2012, respectively.

He is currently a Sr. Project Engineer/Scientist with the Electric Power Research Institute, Palo Alto, CA, USA. In 2009, he was an intern and Midcontinent Independent System Operator. His current research interests include power systems state estimation, protection, stability, operation, control, synchrophasor applications, renewables integration, and smart grid technologies.

Navin Bhatt (F'09) received the M.S.E.E. and Ph.D. degrees in electric power engineering from West Virginia University, Morgantown, WV, USA, in 1975 and 1978, respectively.

He was with American Electric Power (AEP), Columbus, OH, USA, for 33 years, where he conducted, managed, and directed activities related to advanced analytical studies, managed AEP's transmission research and development program, participated in the development of North American Electric Reliability Corporation standards, managed the AEP synchrophasor technology research and development project, and participated in the Eastern Interconnection Phasor Project and North American Synchrophasor Initiative activities. He is a Technical Executive in the Electric Power Research Institute's Grid Operations, and Planning Research and Development area, Loveland, OH, where he focuses on smarter transmission grid and strategic/tactical development and support, as well as technical consultation and management of research and development projects.

Dr. Bhatt is a licensed Professional Engineer in the state of Ohio.